C-A/AP/#273
April 2007

Damping vs. Clamping to Mitigate the RHIC Triplet Oscillations

P. Thieberger, R. Bonati, C. Montag, D. Trbojevic

Collider-Accelerator Department
Brookhaven National Laboratory
Upton, NY 11973

Damping vs. Clamping to Mitigate the RHIC Triplet Oscillations

P Thieberger, R. Bonati, C. Montag and D. Trbojevic

1. INTRIODUCTION

In a recent article [1], C. Montag et.al. compare frequencies observed when studying beam position displacements, with frequencies of mechanical vibrations of the cryostat tank containing the dipoles D0 and the quadrupole lenses Q1, Q2 and Q3. They find agreement for several of the observed frequencies, and they conclude that quadrupole mechanical oscillations, if not mitigated, will affect horizontal beam position stability in ways that will limit future RHIC performance. Using finite element analysis they also compute expected eigenmode frequencies for the oscillatory motions of decoupled cold masses, and they find many lines, some in general agreement with measurements and beam observations.

Here we prefer to concentrate exclusively on the main vibration modes, solely due to the flexibility of the supporting plastic posts. We use a simple model, similar to the one suggested by Montag, et.al. [2]. Understanding these modes and the associated spring constants is important in order to device solutions to this problem. We then use the obtained spring constants to specify stiffeners that will increase the resonant frequencies by factors of 2 or 3, and we estimate the associated heat losses.

Finally we suggest several active damping arrangements that should be very effective in increasing the mechanical stability, incurring negligible heat loss penalties and that appear thus to be preferable to the static support solutions.

2. MECHANICAL OSCILLATION MODES

We adopt the same simple mechanical model used before [2], in which the individual quadrupole magnets are assumed to be rigid cylinders of length **L0** with two elastic suspensions, each located a distance **s** form the center. These elastic suspensions, consisting of ULTEM posts, provide restoring forces against horizontal displacements characterized by certain spring constants **k.** The magnets are assumed to oscillate independently, since the coupling between magnets is week in the transverse direction [1,2]. There are two degrees of freedom for horizontal motions, and correspondingly two oscillation modes. In the “rolling mode” both ends of the cylinder oscillate in phase, while in the “yawing mode” they move with opposite phases. (These are the “dipole” and “quadrupole” modes of reference [2], but we don’t use these terms here to avoid confusion with magnets having the same names.) In both modes the restoring forces are provided by elastic deformations of the ULTEM posts, but the spring constants will be quite different. To see this we consider the two types of deformation illustrated in Figs.1 and 2.

The predominant deformation for the rolling mode will be one where the top flange of the posts are allowed to rotate, while this rotation will not occur in the yawing mode because it would imply twisting the cylinder which is assumed to be rigid to very good approximation. In fact values for these two spring constants where obtained experimentally in 1989 [3]. Figure 3 shows an old sketch of the experimental arrangement. Posts are shown while they are being tested in pairs and therefore the central flange common to both posts moves parallel to the base, and is thus not allowed to rotate. This spring constant determined be measuring deflection as function of applied force is relevant to our yawing oscillation One of the posts was then

removed and the deformation as function of applied force was again measured to get an approximate value of the spring constant relevant to our rolling mode. The values obtained are 60,000 lb/inch for the yawing mode (also used in [2]) and between 30,000 and 35,000 lbs/inch for the rolling mode [3].

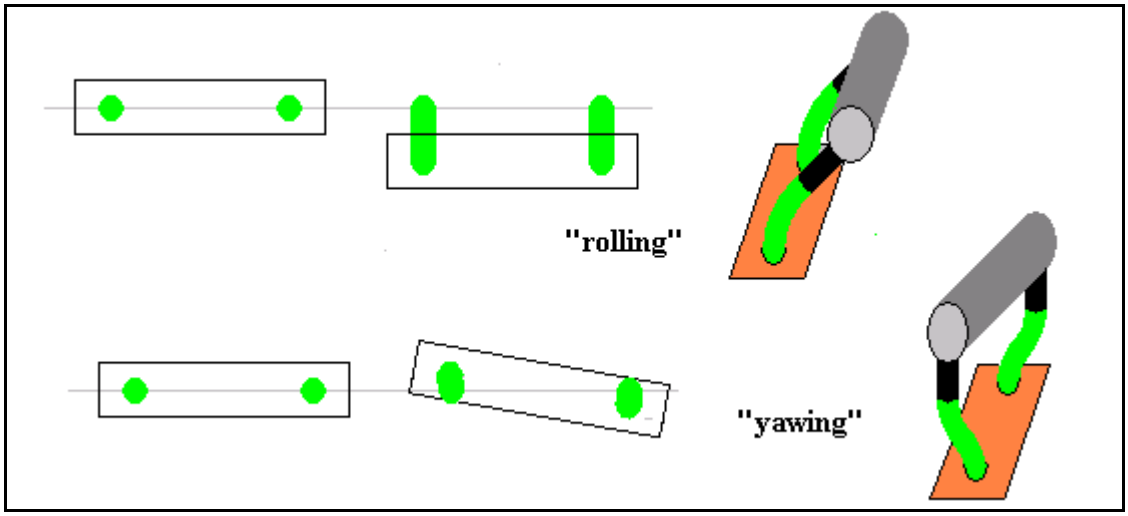

Fig. 1 Schematic representation of the two main oscillation modes.

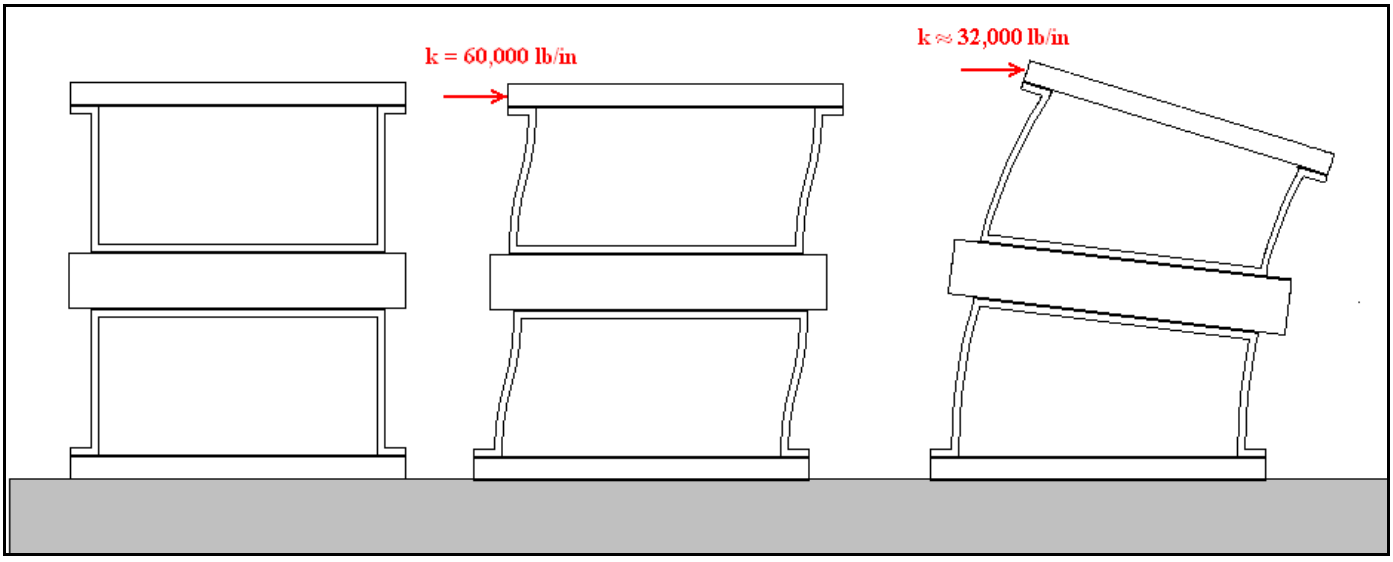

Fig. 2 ULTEM post assemblies shown un-deformed to the left, and deformed in the middle and to the right where the upper surface is respectively constrained or not constrained to remain parallel to the base. Respective measured spring constants are indicated.

In the yawing mode, since there is no rotation around the longitudinal cylindrical axis, the restoring forces will only depend on the horizontal deflection, and not on the vertical position of the oscillating object. This is not true for the rolling mode, where the restoring forces transmitted to the center of mass of the object will

depend of the height of that center-of-mass. This is illustrated in Fig.4 where we also show the simple equations used to obtain the effective spring constant corresponding to the center-of-mass height.

Strictly speaking the rolling oscillation is better represented by a rotation around a line through the center height of the posts, and the restoring forces represented by the spring constant are transformed into restoring torques. Frequency calculations were carried out both ways and the results were similar differing only by 3 or 4%. The more accurate values, obtained with the second method are the ones shown in Table 1.

Table 1

Lens	Calculated frequency for the rolling oscillation(Hz)	Calculated frequency for the yawing oscillation (Hz)
Q1	7.8	16.3
Q2	5.2	14.5
Q3	5.6	14.5

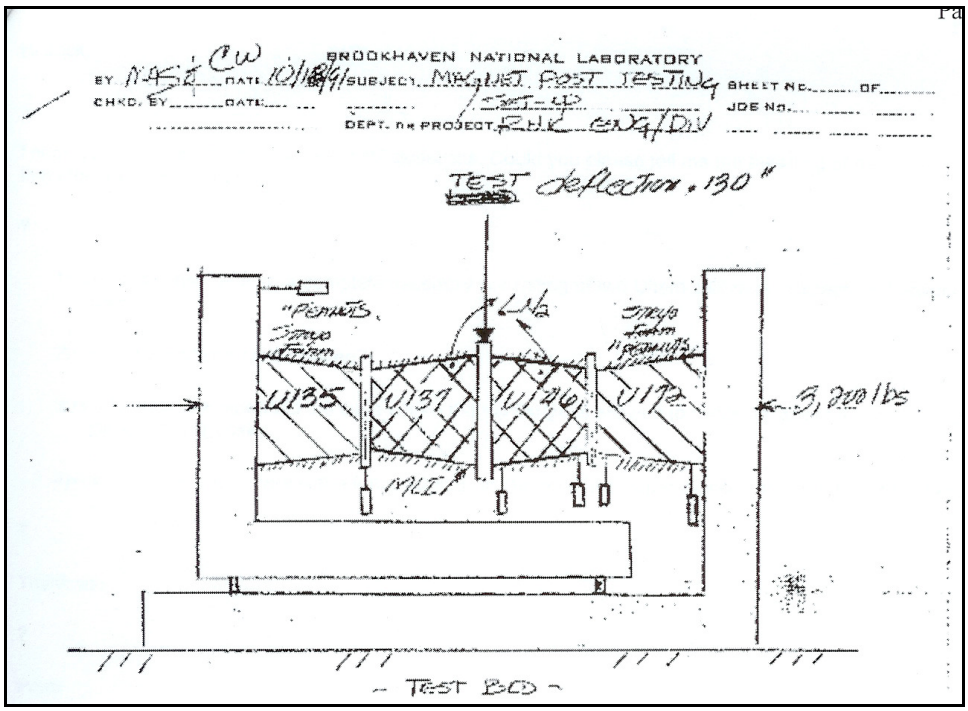

Figure 3 1989 sketch showing the arrangement used to measure the spring constant of the ULTEM posts. One of the posts was removed to measure the spring constant when the end of the post is free to rotate.

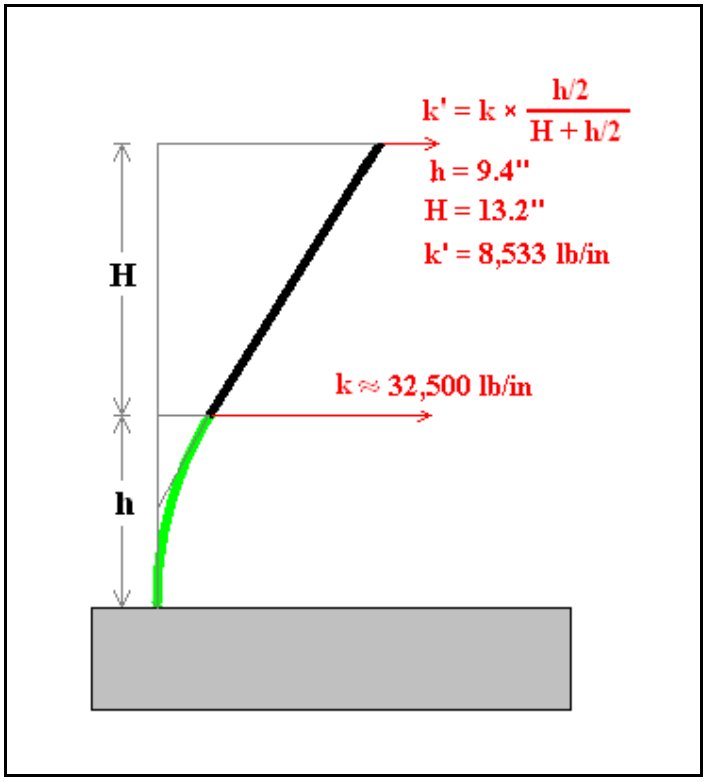

Fig. 4 Simplified schematic representing the flexible post of height h (green) connected to a rigid support of height H, where h + H is the height of the center of mass. The effective spring constant k' corresponding to the center of mass position is calculated from spring constant k measured at the top of the post.

The frequencies in table 1 are now compared with the beam motion frequency spectrum taken from [1] and the results are shown in Fig. 5

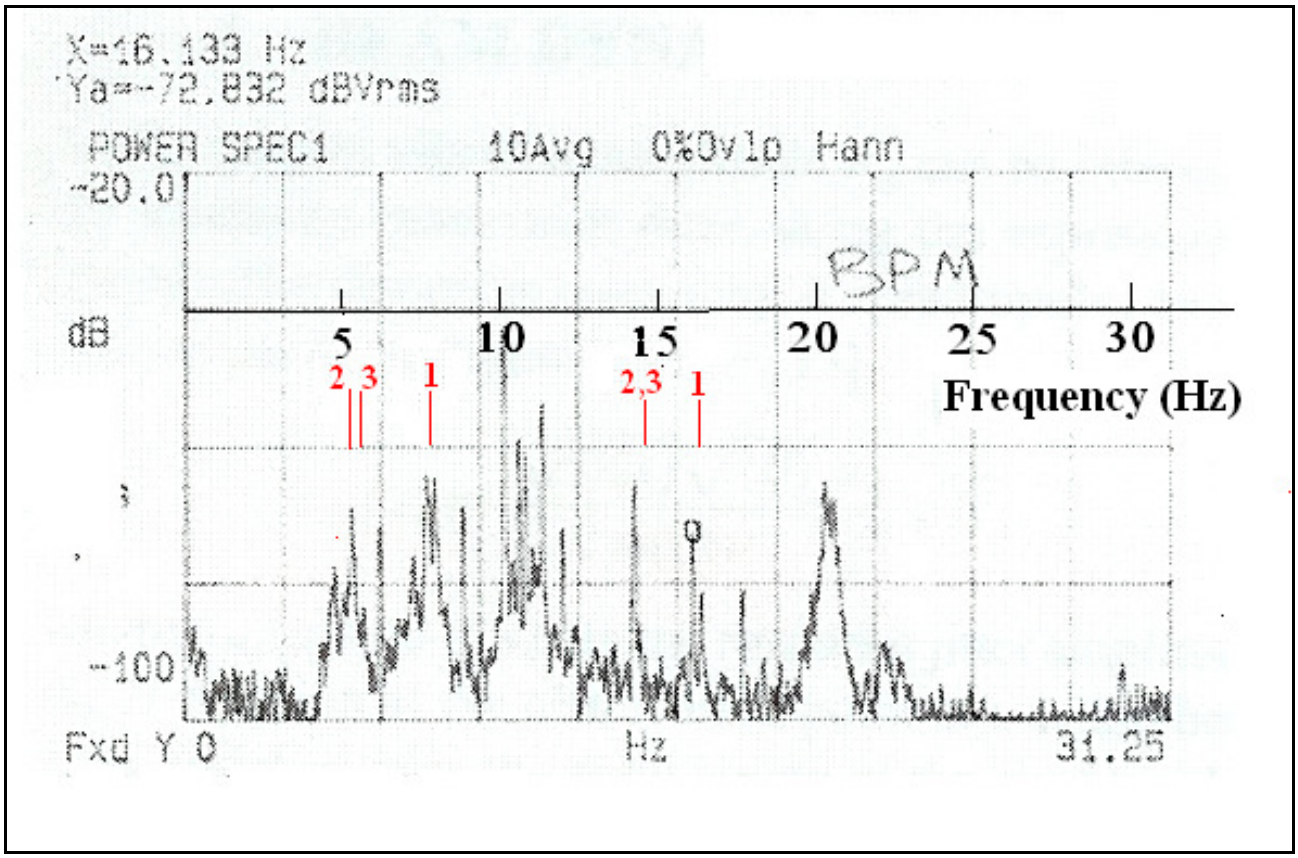

Fig. 5 Frequency spectrum encountered in the BPM data [1] compared to the frequencies predicted here for the two main oscillation modes of Q1, Q2 and Q3. The red lines numbered 1,2,3 at the center of the figure correspond to the expected yawing-mode oscillations and the lower frequency ones to the left are for the rolling mode.

There is fairly good agreement for all of the lines, including the lowest observed frequencies. But there are more lines in the beam spectrum suggesting that either sources other than quadrupole lens vibrations may also perturb the beam or that the hypothesis of independent motion for the individual cold masses may not be a very good approximation. There is some experimental evidence for this last possibility from observed frequency spectra [6] measured with an accelerometer attached to one of the magnets while coupled to the neighboring ones.

In the following sections, we briefly discuss ideas for passive and active methods that may be considered to effectively reduce the vibration amplitudes by counteracting the effects of the driving forces. Identifying and reducing the driving forces is of course another approach, but this possibility is not addressed here.

3. MITIGATION BY STIFFENING THE SUPPORTS

Stiffening or supplementing the mechanical supports of the magnet will increase the resonant frequencies. To understand the effects of increasing the resonant frequencies we write down the steady-state solutions for a driven damped harmonic oscillator of mass ***M***, spring constant ***k*** and "quality factor" ***Q***. In equation 1, ***F(f)*** is the amplitude of a driving force of frequency ***f***, producing a steady-state oscillation amplitude ***A(f)***, where the resonant frequency f_0, is given by equation 2

$$A(f) = \frac{F(f)}{4\pi^2 \times M \times \sqrt{(f^2 - f_0^2)^2 + f_0^2 f^2 / Q}} \qquad 1)$$

$$f_0 = \frac{1}{2\pi} \times \sqrt{\frac{k}{M}} \qquad 2)$$

And at resonance:

$$A(f_0) = \frac{F(f_0) \times \sqrt{Q}}{4\pi^2 \times M \times f_0^2} \qquad 3)$$

If there are forces present of various frequencies then the total amplitude is obtained by summing or integrating the amplitude contributions given by 1) taking into account the correct phases.

For a "white" spectrum of driving frequencies (***F(f)*** = constant) we see from 3) that the resonant amplitudes will be reduced quadratically as the resonant frequency is increased, but, according to 2), only linearly with respect to the corresponding increases in the spring constant.

With an unknown driving force spectrum, one can not predict how the vibration amplitude will change when stiffening the structure. On the one hand the result may be much better than indicated above if one moves the resonant frequencies away from predominant driving frequencies, but it may also be worse if the opposite happens.

We will use Q2, the heaviest magnet, as an example of what it would take to increase the resonant frequencies, and we will consider the arrangement shown in Fig. 6. Two tie-rods are fastened to the top of each end of a Q2 magnet, and are connected to pre-tensioning devices attached to a rigid frames supported from the tunnel floor. The rods either traverse and are welded to the end-flanges of two small bellows, or they are otherwise attached so as to preserve the integrity of the insulating vacuum. Tension is applied when the magnet is cold by rotating the threaded support-caps, perhaps using load cells (not shown) as guidance. When the magnet warms up, thermal expansion will remove the tension and the rods are free to move into the support cavity, as indicated at the top of the drawing. There will be an arrangement such as the one shown in Fig. 6 close to each end of the magnet.

We considered stainless steel and G10 as possible materials for these rods. The room-temperature elastic modulus (Young's modulus) for 304 SS is 2.1E11 Pa and 1.72E10 Pa for G10. We use room temperature values for our calculations without taking credit for the increased stiffness (by some ~ 30% at 4^0K [3]) that will increase the spring constants slightly when a portion of each rod is at cryogenic temperatures. However a room temperature approximation can not be used for the thermal conductivity that changes drastically as shown in Fig. 9 [4]. We choose the cross-sections of these rods to provide equal spring constants, and therefore the cross sections of the longer rods will be larger. The lengths of the rods shown in Fig. 5 are 690 mm and 320 mm.

The equivalent spring constant for the rolling mode before installing the tie-rods, calculated now at the top of the magnet where the tie-rods are fastened is 6,100 lb/in, while it is reduced to 40,000 lb/in for the yawing mode from the previously discussed value of 60,000lb/in by locating the tie-rods closer to the end of the magnet than the post locations. These are the spring constant values that will be incremented by the presence of the tie-rods, and the resonance frequencies will increase accordingly. The results of these calculations are shown in Figs. 7 and 8.

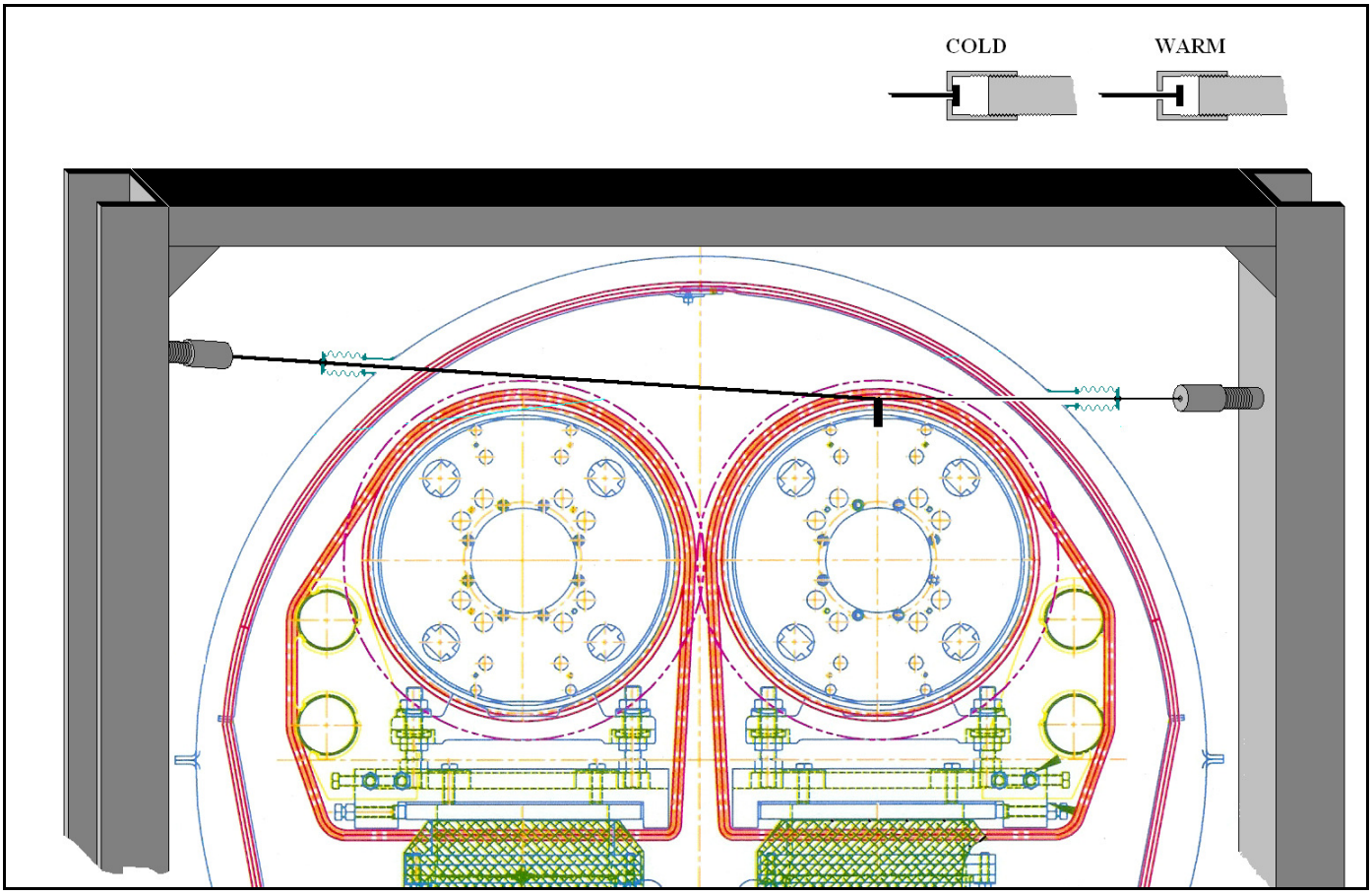

Fig. 6 Tie-rod system to increase the resonant frequency. Two arrangements as the one shown here would be used per magnet, one located close to each end.

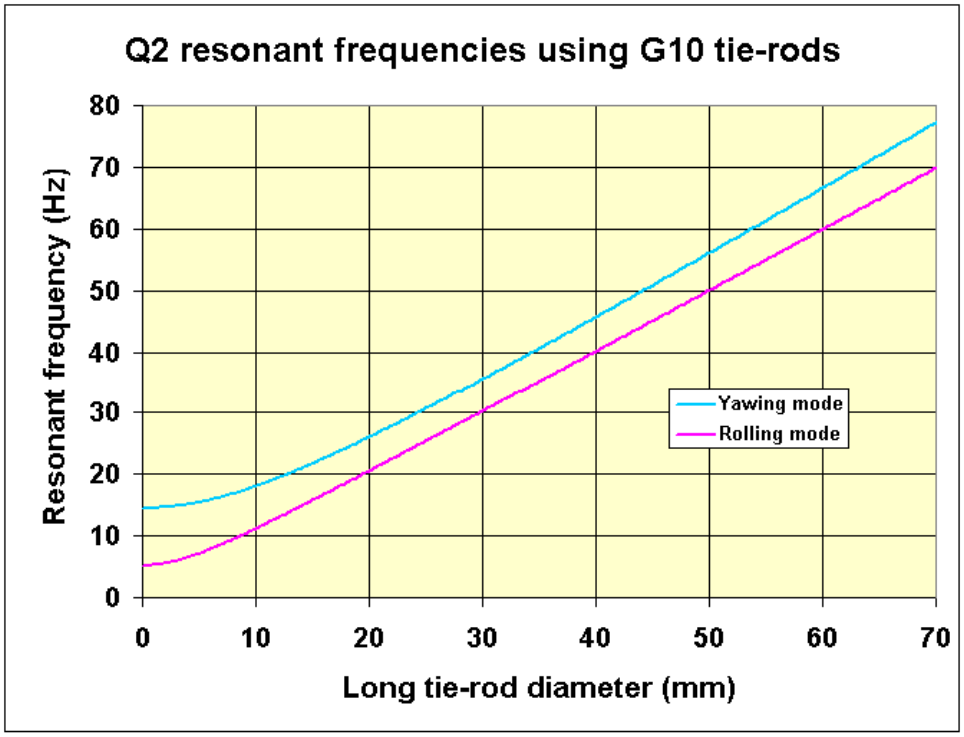

Fig. 7 The diameters of the short tie-rods are 68% of the long tie-rod values.

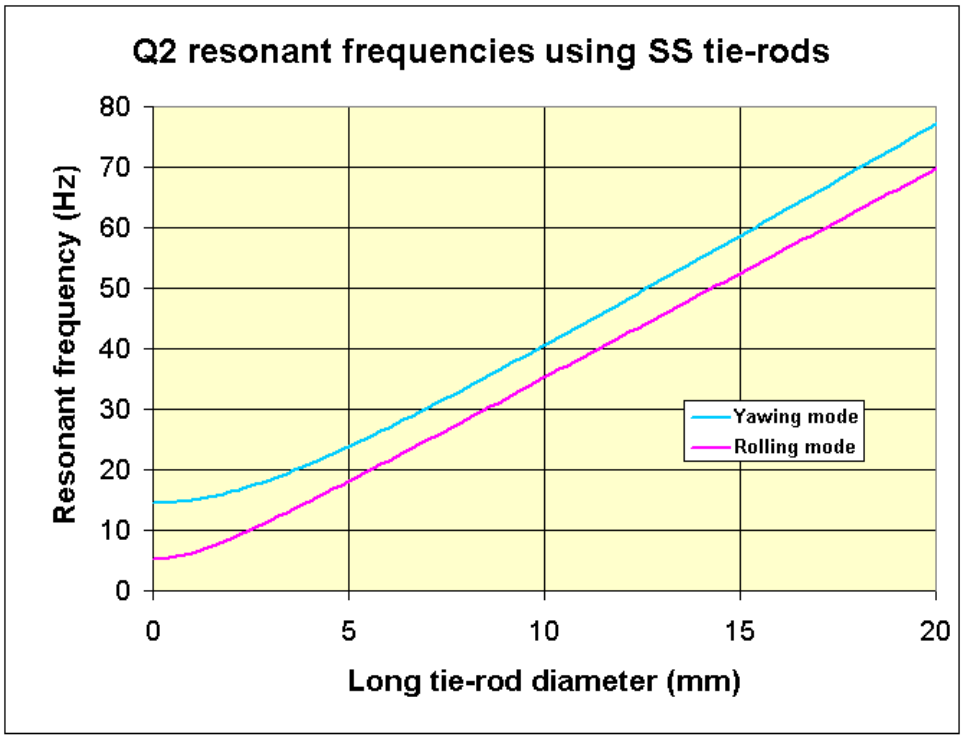

Fig. 8 The diameters of the short tie-rods are 68% of the long tie-rod values.

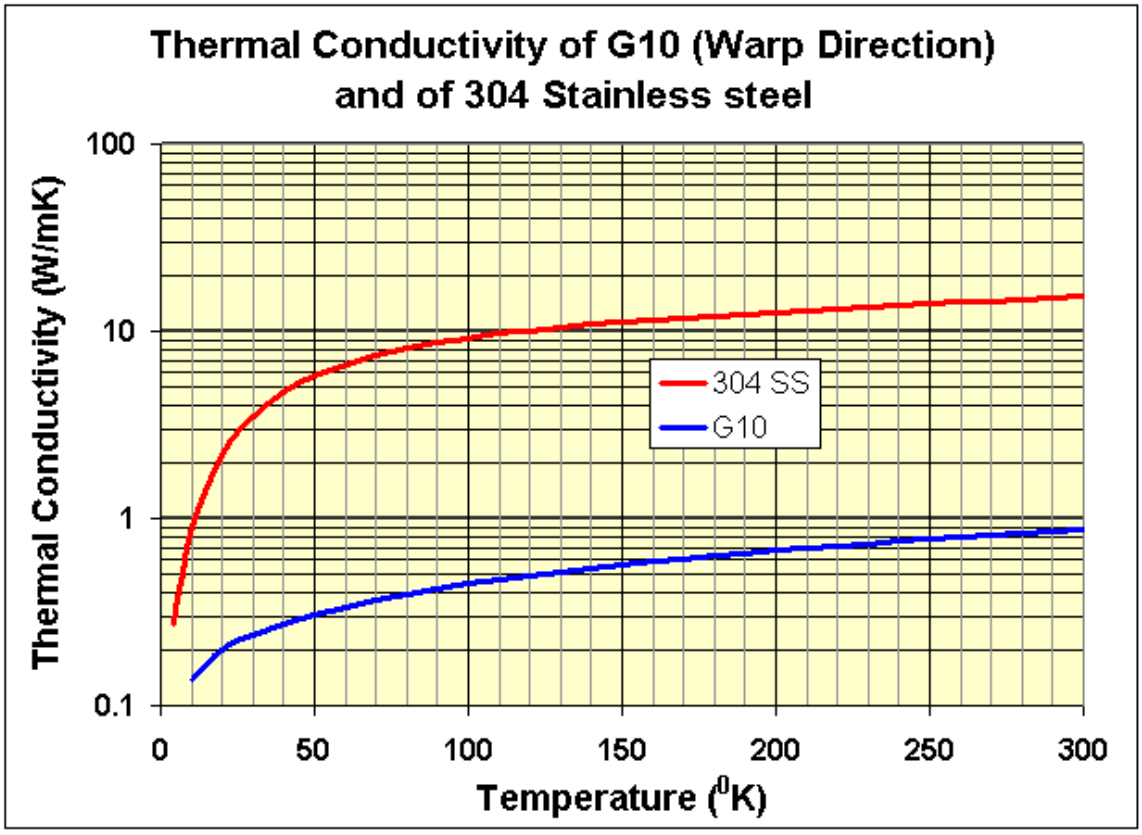
Thermal Conductivity of G10 (Warp Direction)
and of 304 Stainless steel
Thermal Conductivity (W/mK)
100
10
1
0.1
0
50
100
150
200
250
300
Temperature (^{0}K)
304 SS
G10

Fig . 9

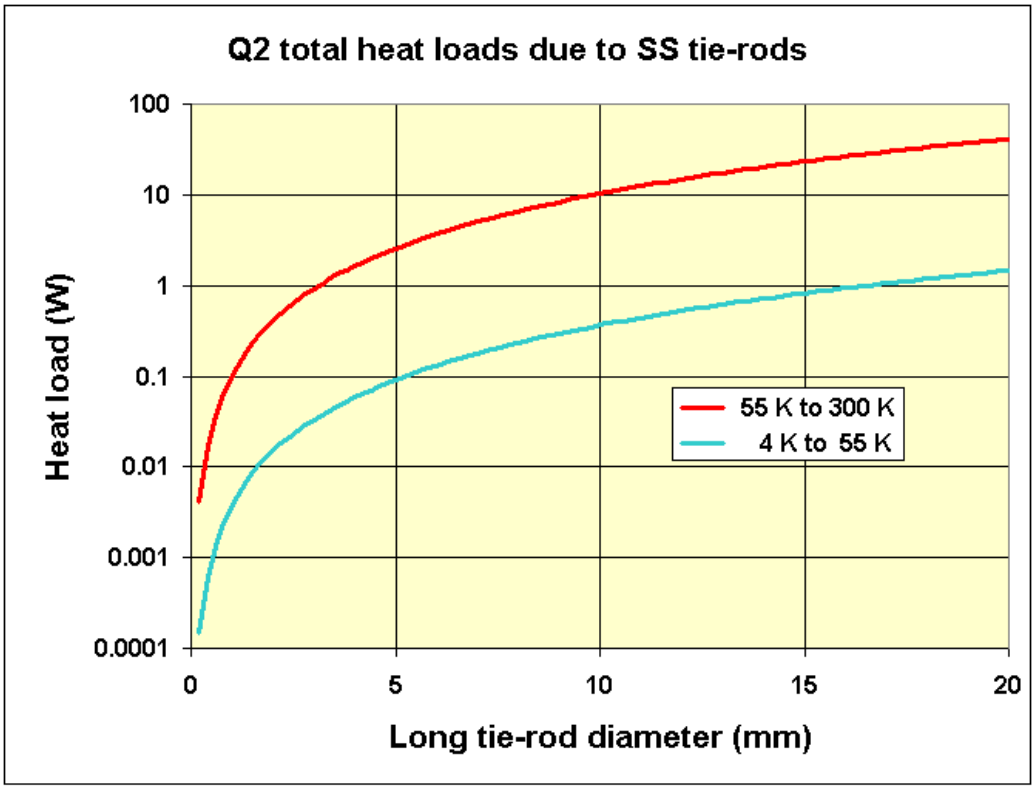
Q2 total heat loads due to SS tie-rods
Heat load (W)
100
10
1
0.1
0.01
0.001
0.0001
0
5
10
15
20
Long tie-rod diameter (mm)
55 K to 300 K
4 K to 55 K

Fig. 10

Figure 10 shows the heat load results for stainless steel obtained by using the thermal conductivity data [4] shown in Fig.9. Similar plots can be generated for other materials such as G10. Heat losses will be smaller for G10 for equal resonant frequency increments.

While heat loads may be tolerable for significant stiffening of the magnets, it is not entirely clear by how much the resonant frequencies need to be increased, as was discussed above. Also the rigid support frame shown in Fig. 6 needs to be quite massive to provide the required rigidity. We want to increase the present effective spring constants, which are of the order of 60,000 lb/in by at least a factor 10 without being limited by the support structure. Therefore the spring constant of this structure, measured at the height of the tie-rod connections will need to be at least 10^6 lb/in.

4. MITIGATION BY DAMPING

Passive or active damping seem to be a good alternatives because more attenuation can be achieved, at least in principle, and because of the above mentioned uncertainties about the effects of increasing the resonant frequencies without knowing the driving frequency spectrum. More importantly the forces involved will be much smaller, thus allowing much thinner rods (or wires) and much weaker supports. The result will be less heat load and cheaper implementation.

To estimate the magnitude of the damping forces we use 3) to find the amplitude of the driving force that will cause a certain vibration amplitude at resonance. The required damping forces (at that frequency) should have the same amplitude.

$$F(f_0) = \frac{4\pi^2 \times A(f_0) \times M \times f_0^2}{\sqrt{Q}} \qquad 4)$$

For the 5.2Hz rolling oscillation of the 3110 Kg Q2 mass, assuming an amplitude A = 10μm and Q=100 we get a 3.1 Newton force amplitude or 0.69 lb force. Much higher values of Q have been reported [5] leading to even smaller forces. Therefore only very thin wires need to be used, instead of the ~½" thick tie-rods considered before. Also, the forces are so small that there is no good reason for balancing them pulling from both sides. The systems suggested in this section all consist of pairs of sensors, actuators or dampers, all located on a single side of each magnet, and close to its ends.

Heat-load consideration will not be a large factor in designing these systems. Even for e.g. 1 mm diameter 304 SS wires, which have a yield strength of ~50 lb, and are therefore probably thicker than necessary, the heat loads per magnet will only be ~0.02 W and ~ 0.5 W from 4^0 to 55 ^{0}K and from 55^0 to 300 ^{0}K, respectively for a geometry similar to the right side of Fig. 6, and using four wires per magnet.

4.1 Passive damping

Passive damping systems are the more effective the large the Q-values are. The Q-value can then be easily reduced by a large factor resulting in considerable attenuation as can be seen from Eq. 3. Figure 11 schematically shows an example of such a system where the energy-dissipating device has been located outside of the vacuum. The problem is that so far we have not been able to find a commercial "shock absorber" type of device adequate for this application.

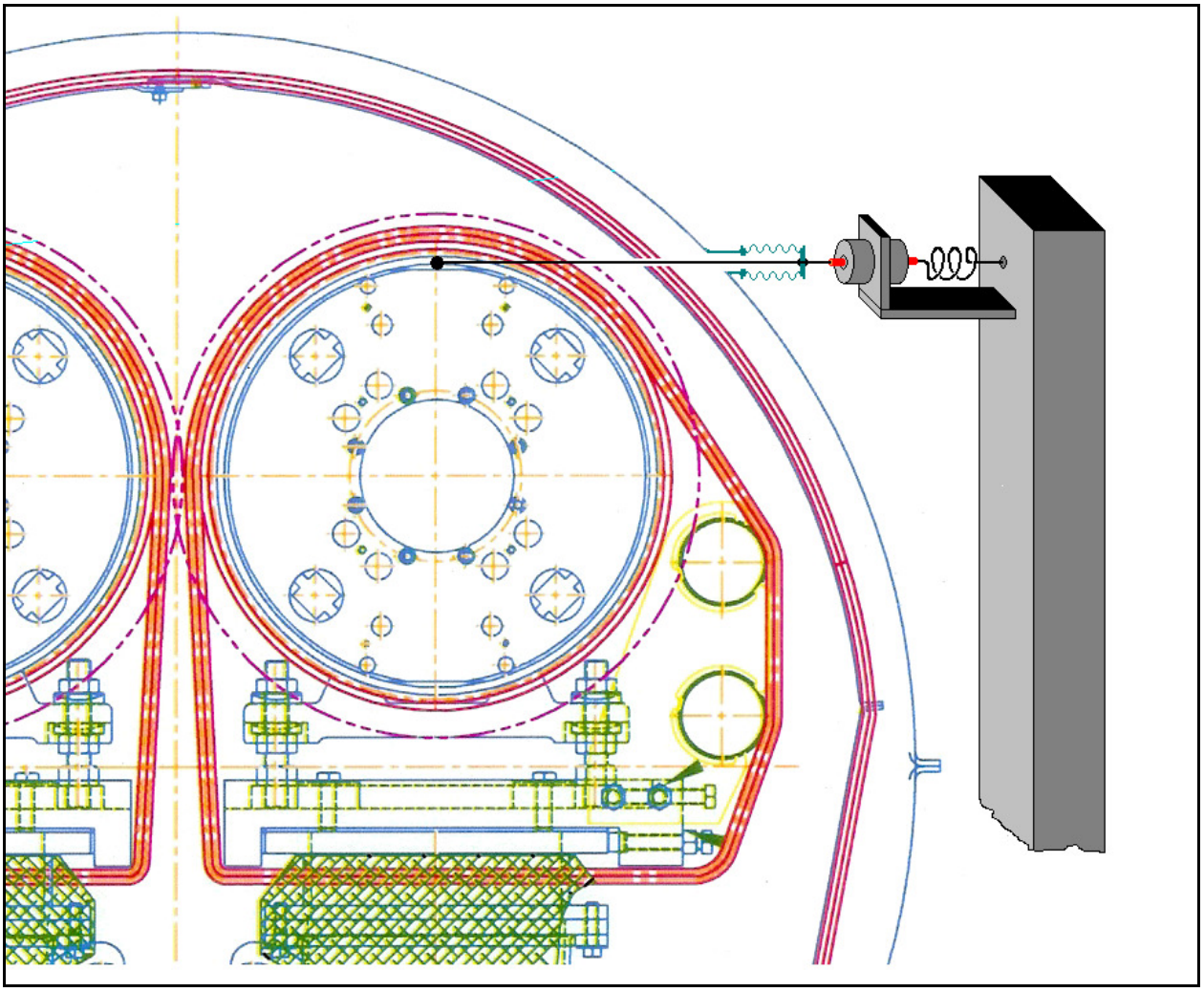

Fig. 11 Example of passive damping system using a linear shock absorber. The spring attached to the vertical support must be strong enough to keep the wire taut by overcoming the pressure-induced force on the small bellows flange.

A 1 mm diameter stainless steel wire would be more than adequate to couple the cold mass to the shock absorber for the forces estimated in the previous section, which were based on a hypothetical Q-value of 100 and driving forces close to the resonance frequency. It is unlikely that a larger diameter wire will be required, but further measurements and tests would be required to be sure.

4.2 Active Damping

In this section we sketch in a qualitative way several possible configurations for sensing magnet motions to actively feed back damping forces. Research of available transducers, sensors and actuators, and detailed calculations and tests will be required to estimate performance and costs. The conceptually simplest systems are those where the wires used for sensing and those used for driving are kept separate to avoid having to contend with signal components due to variable wire stretching. Such are the systems illustrated by Fgs 12 through 14 below; with pairs of sensing and driving wires located close to each end of the magnet. At the end (Fig. 15) we briefly touch on the possibility of combining sensing and driving wires.

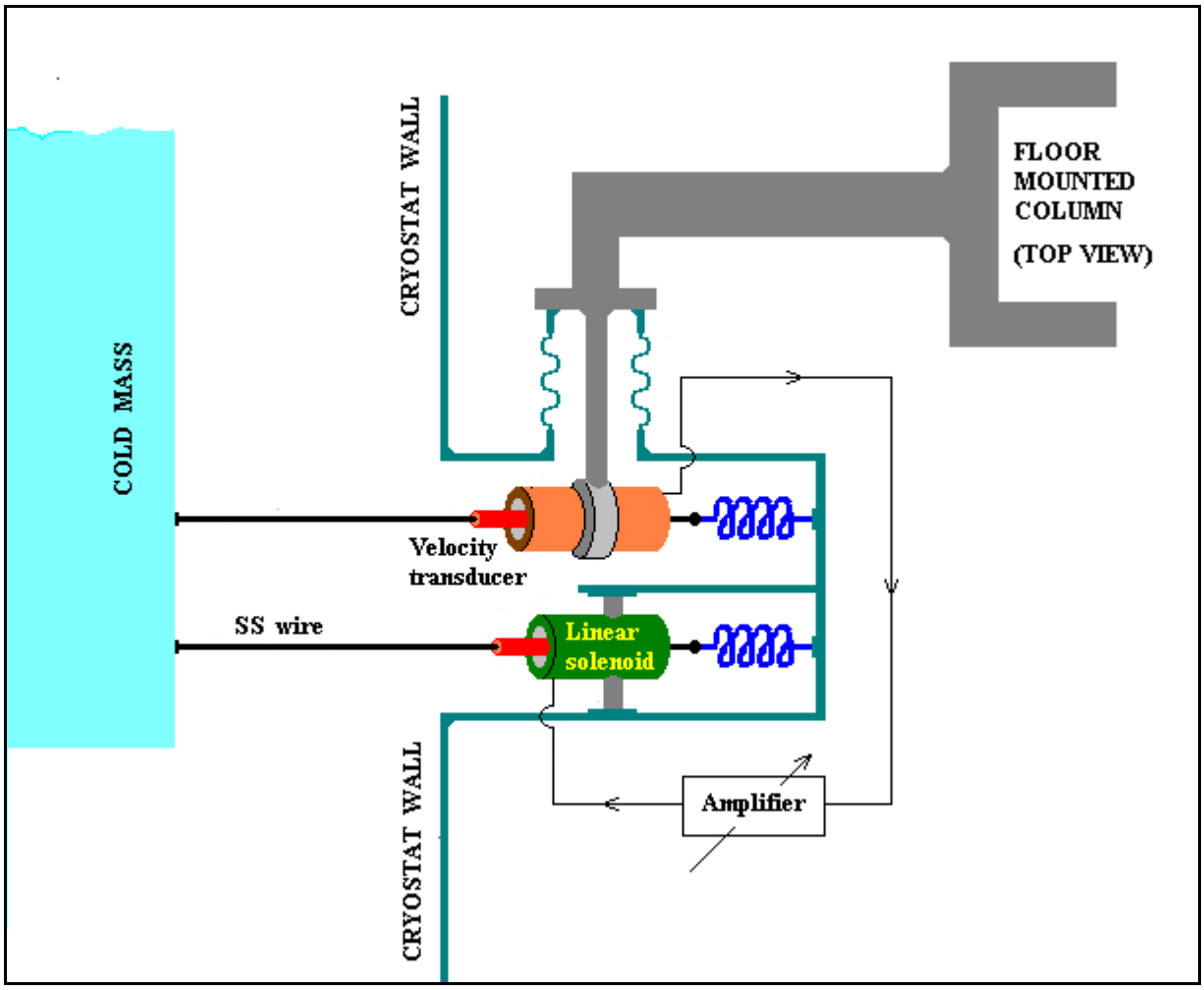

Fig 12 Active feedback system where a damping force proportional to the velocity is generated by amplifying the signal from velocity transducer. The springs have sufficient strength and length to always keep the wires taut, under all conditions of cryostat temperatures and linear solenoid generated forces. The stationary part of the velocity transducer is supported, through a bellows, by means of a floor-mounted column. This is a much weaker and cheaper structure than the frame shown in Fig. 6. A system similar to the one shown here can be designed by replacing the velocity transducer by a linear position transducer, and using a signal differentiating stage before the amplifier to generate the velocity signal.

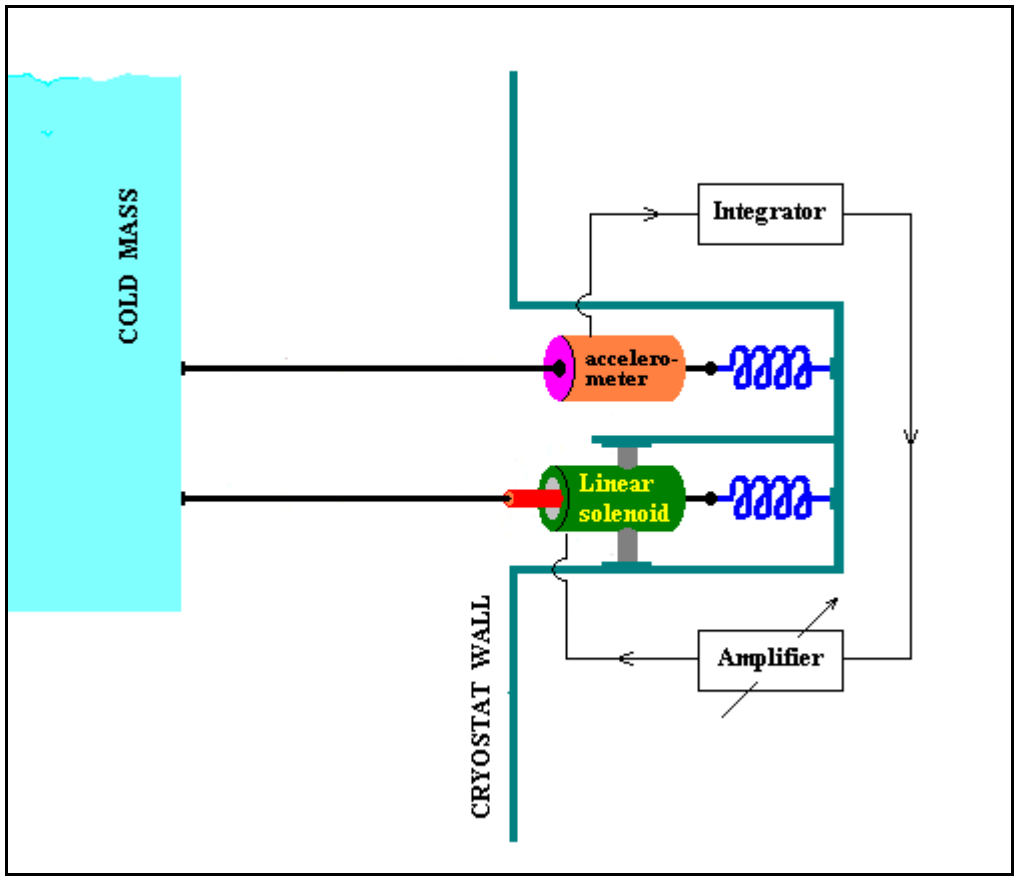

Fig. 13 Active feedback system where a damping force proportional to the velocity is generated by integrating the accelerometer signal. The springs have sufficient strength and length to always keep the wires taut under all conditions of cryostat temperatures and linear solenoid generated forces. Advantages of this system are that no floor-mounted support is required and that commercially available compact accelerometers are probably suitable for this application.

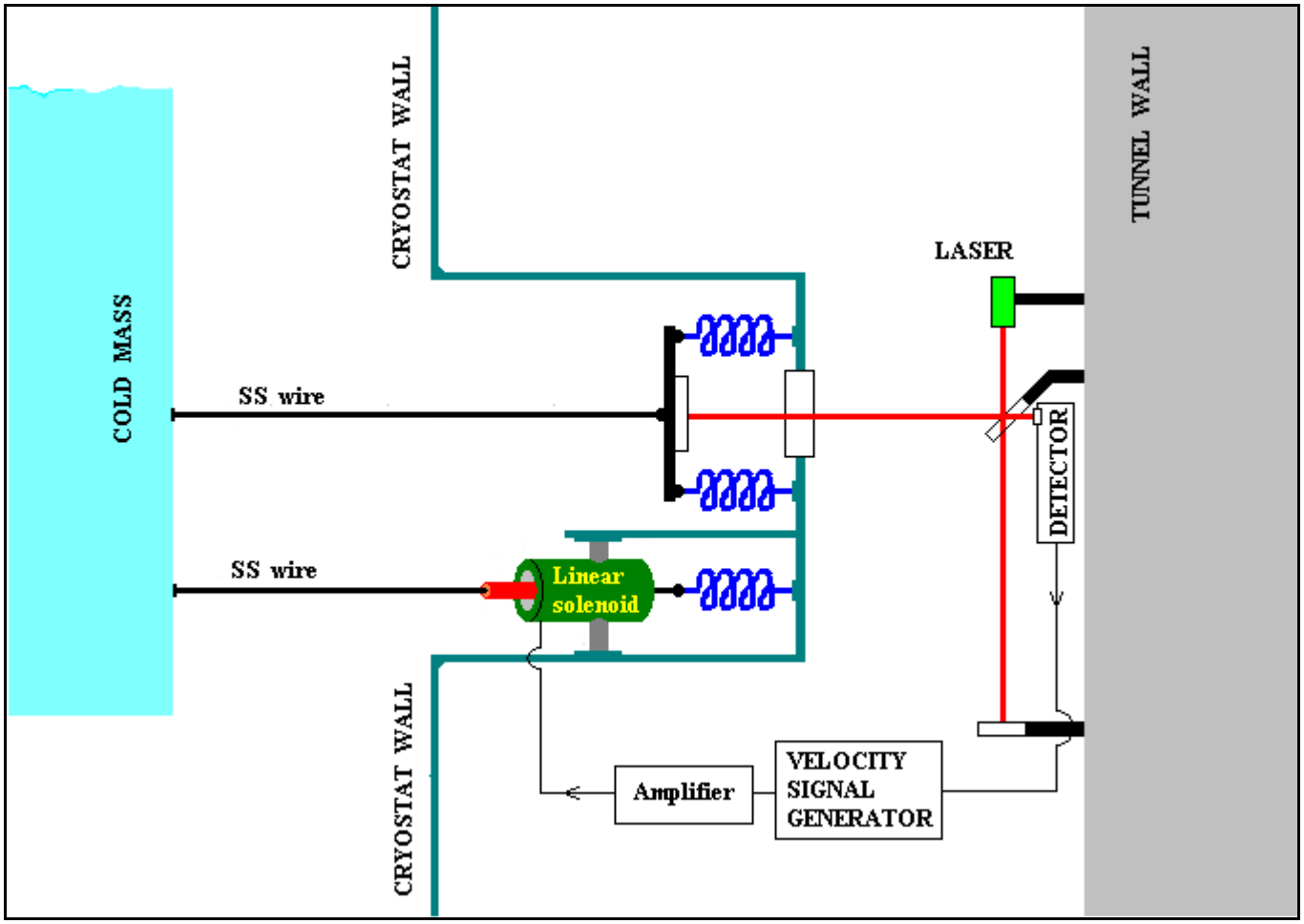

Fig. 14 Active feedback arrangement where a damping force proportional to the velocity is generated using a Michelson interferometer that uses the wall of the tunnel as position reference. This system is no doubt superior to the ones described above, but it is probably much better than required and too expensive.

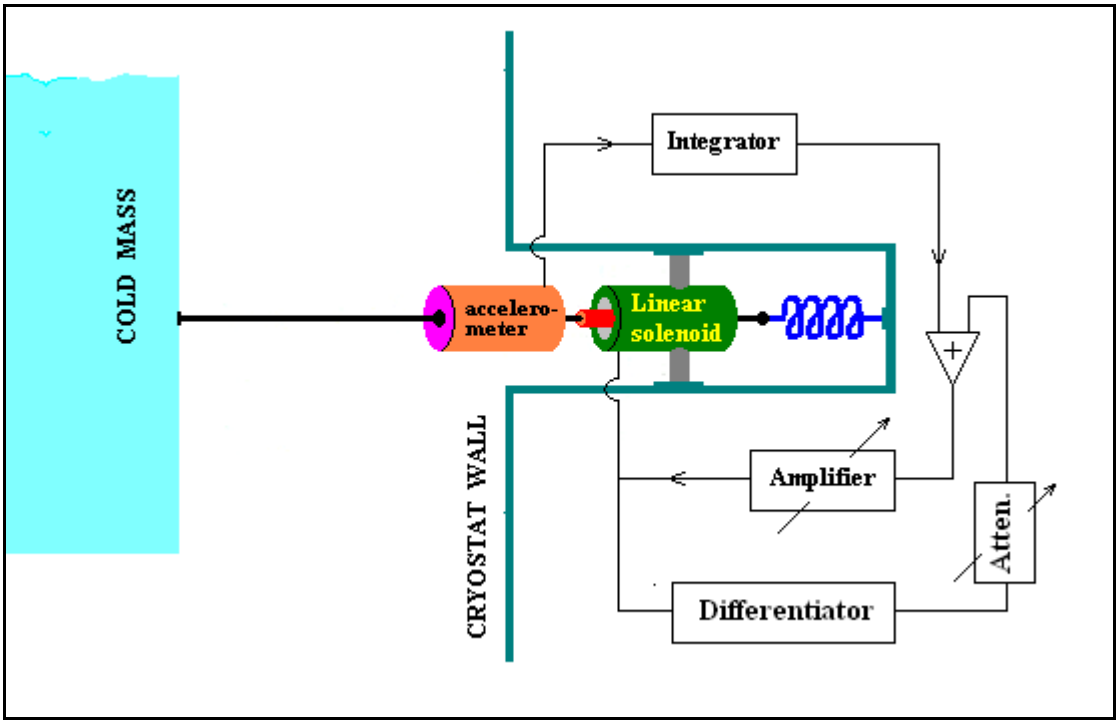

Fig 15 Active feedback system similar to the one of Fig 13, where a damping force proportional to the velocity is generated by integrating the accelerometer signal, but using a single wire. This wire can now have a cross section twice as large as before for the same heat loads. If nevertheless, stretching of the wire is still significant, electronic compensation can be applied by differentiating the force signal that is proportional to the elongation. This differentiated signal is then proportional to the speed of elongation and is added with the correct sign so as to cancel its effect on the velocity signal.

We should note that for all the active feedback systems except the last one (Fig. 15), elastic stretching of the wires is of no concern since motion sensing is independent of such stretching as long as the spring constant of the tensioning spring is much smaller than the wire's spring constant. For the case of Fig. 15, wire stretching is electronically compensated, but may in principle become a limiting factor if the required compensation becomes too large. Because of the same considerations mentioned in section 4.1, this is not expected to be the case for 1 mm diameter stainless steel wires.

It should also be noted that the electronic circuits shown as simplified block diagrams in figs 12 through 15 will in reality be somewhat more complicated since the usual band-pass and/or low-pass filters will be required to prevent high frequency oscillations.

Both interferometer-based and accelerometer-based systems are being considered at SLAC for damping vibrations of the last lens preceding the Linear Collider interaction point where the beam size will be ~1nm. At the LIGO project such techniques are pushed even much further. That is the state of the art. We are aiming for a 0.1 mm beam sizes and are concerned about 1 μm vibrations. It shouldn't be too difficult or too expensive to solve this problem.

We conclude that the active damping schemes, especially the one of Fig.13, offer a very attractive alternative to possible solutions based on stiffening the supports. The heat loads are much smaller, the results will be better, and the implementation is probably easier and cheaper.

REFERENCES

1) C. Montag, R. Bonati, J.M. Brennan, J. Butler, P. Cameron, G. Ganetis, P. He, W. Hirzel, L.X. Jia, P. Koello, W. Louie, G. McIntyre, A. Nicoletti, J. Rank, T. Roser, T. Satogata, J. Schmalzle, A. Sidi-Yekhlef and T. Tallerico, NIM A 564 (2006) 26-31.

2) C. Montag, M. Brennan, J. Butler, R. Bonati, P. Koello, "Observation of Mechanical Triplet Vibrations in RHIC", Proc. 26th Advanced ICFA Beam Dynamics Workshop on Nanometre Size Colliding Beams (NANOBEAM) 2002, CERN-Proceedings-2003-001

3) John Sondericker, private communications.

4) Cryogenic Data Handbook, http://www.bnl.gov/magnets/Staff/Gupta/cryogenic-data-handbook/Section7.pdf

5) Mike Blaskiewicz, private communication.

6) G. Ganetis, private communication.